ISCI, Volume *3*

Supplemental Information

Mitochondria-Targeted Honokiol Confers a Striking Inhibitory Effect on Lung Cancer via Inhibiting Complex I Activity

Jing Pan, Yongik Lee, Gang Cheng, Jacek Zielonka, Qi Zhang, Martina Bajzikova, Donghai Xiong, Shirng-Wern Tsaih, Micael Hardy, Michael Flister, Christopher M. Olsen, Yian Wang, Ole Vang, Jiri Neuzil, Charles R. Myers, Balaraman Kalyanaraman, and Ming You

Supplementary Materials List

Transparent Methods

Supplementary Materials and Methods

Fig. S1. [Synthesis of mitochondria-targeted honokiols (mito-honokiols)], Related to Fig. 1

Fig. S2. [NMR spectra of synthesized compounds 1, 2+3 and 4], Related to Fig. 1

Fig. S3. [HPLC analysis of mitochondria-targeted analogs of honokiol], Related to Fig. 1

Fig. S4. [Mito-HNK inhibits invasion without induction of significant cell death in lung cancer cells], Related to Fig. 3

Fig. S5. [Experimental setup for measurement of mitochondrial complex I and II activities in permeabilized cells], Related to Fig. 4

Fig. S6. [The effect of HNK and Mito-HNK (24 h treatment) on cellular ROS production], Related to Fig 4

Fig. S7. [Effect of Mito-HNK on the oxidation status of cytosolic (Prx1) and mitochondrial (Prx3) peroxiredoxins in three different lung cancer cell lines], Related to Fig 4

Fig. S8. [Role of STAT3 in the anti-proliferative and anti-invasive effects of HNK and Mito-HNK in small cell lung cancer cells], Related to Fig 6

Fig. S9. [Generation and validation of the STAT3 knockout H2030-BrM3 cell line], Related to Fig 6

Fig. S10. [Eliminating mtDNA with Herpes simplex virus UL12.5 abrogates the anti-proliferative effects of Mito-HNK in lung cancer cells], Related to Fig 5

Fig. S11. [Combination of Mito-HNK with cisplatin increased anti-proliferative effects in lung cancer cells], Related to Fig 3

Table S1. [Modified Irwin screen after 8-week Mito-HNK treatment], Related to Fig. 1

Table S2. [Gene expression in malignant tumor cells from brain metastatic lesions], Related to Fig 7

Table S3. [Gene expression in nonmalignant stromal cells from brain metastatic lesions], Related to Fig 7

Transparent Methods

Materials and Methods

Cell culture and reagents

The brain metastatic lung cancer cell lines H2030-BrM3 and PC9-BrM3 were generous gifts from Dr. Joan Massage (Memorial Sloan Kettering Cancer Center, New York, NY). H2030 and PC9 cell lines were established from lung adenocarcinoma patients; H2030 has a *KRAS*^{G12C} mutation (*76*) and PC9 has an EGFR$^{\Delta exon19}$ mutation (*77*). H2030-BrM3 and PC9-BrM3 cells are sublines that consistently form brain metastasis in 100% of animals compared to a 10% efficiency of the parental lines (*39*). These cells were engineered to stably express a green fluorescent protein (GFP)-luciferase fusion protein. The small cell lung cancer cell line DMS-273 was purchased from Sigma-Aldrich (St. Louis, MO). The DMS-273 cell line was established from the pleural fluid cells of an SCLC patient, who relapsed from both chemotherapy and radiotherapy, and was classified as variant SCLC, with a fast growth rate and high metastatic potential (*78*). The PC9-BrM3 and H2030-BrM3 cell lines were maintained in RPMI-1640 medium (11875-093, Gibco) supplemented with 10% fetal bovine serum (FBS) (Invitrogen, Carlsbad, CA). DMS-273 cells were maintained in Waymouth's medium (11220-035, Gibco) supplemented with 10% FBS in a 37°C humidified 5% CO_2 incubator. 143B and 143B ρ0 cells were a gift from by Dr. Ole Vang, Department of Science and Environment; Roskilde University, Denmark; B16 and B16 ρ0 cells were generously provided by Dr. Martina Bajzikova, Institute of Biotechnology, Czech Academy of Sciences, Czech Republic. Both 143B and B16 cells were cultured as previously

described in DMEM (11965-092, Gibco) supplemented with 10% FBS, sodium pyruvate (1 mM) and uridine (50 µg/ml).

Honokiol was purchased from Sigma-Aldrich (St. Louis, MO). We synthesized mono- and bis-substituted HNK molecules as shown in **Fig. 1** using a procedure described in the **Supplementary Materials**. The mono-substituted honokiol derivative (Mito-HNK) has been isolated as a mixture of two isomers (**Supplementary Fig. 1**), while only one double-substituted analog (bis-Mito-HNK) was obtained. The products were isolated on gel chromatography and purified by preparative high performance liquid chromatography (HPLC). The structure identity was confirmed by nuclear magnetic resonance (NMR) (**Supplementary Fig. 2**) and high resolution mass spectrometry. The purity of the compounds was rigorously tested before use by HPLC analyses (**Supplementary Fig. 3**).

Cell proliferation assay

Cells were seeded in 96-well tissue culture plates at 1,000–3,000 cells per well. Twenty-four hours after seeding, cells were exposed to various concentrations of Mito-HNK, whereas control group cells received fresh medium with an equivalent amount of dimethyl sulfoxide (DMSO) vehicle. Plates were incubated at 37°C under 5% CO_2 and monitored using the IncuCyte Live Cell analysis system (Essen Bioscience, Ann Arbor, MI). The IncuCyte™ Live-Cell Imaging Analyzer provides real-time cell confluence data, which were analyzed using the IncuCyte 2011A software. All assays were performed in triplicate or quadruplicate.

Transwell invasion assay

Boyden chamber transwells pre-coated with growth-factor-reduced Matrix were purchased from Fisher Scientific (Pittsburgh, PA). Transwell invasion assays were performed as described by the manufacturer's protocol. Briefly, $2–3\times10^5$ cells were seeded into each transwell, filled with serum-free culture medium. The bottom wells were filled with cell culture medium or Waymouth's medium with 10% FBS and either HNK or Mito-HNK. Controls received an equivalent amount of DMSO. After 36 hours, cells were fixed with 10% formalin and stained with 5% crystal violet in 70% ethanol. Invaded cells were counted at a magnification of 10× in three randomly selected areas of each transwell, and the results were normalized to the control.

Toxicity studies of Mito-HNK

All animal procedures were performed in accordance with the Medical College of Wisconsin Institutional Animal Care and Use Committee. An eight-week subchronic toxicity study was conducted in A/J mice. A Modified Irwin Screen was used employing 35 distinct measurements to assess sensorimotor, neurological, and autonomic nervous system function. A/J mice were treated with vehicle control or Mito-HNK, given *via* oral gavage five days per week for eight weeks. During treatment, the modified Irwin Screen was conducted at baseline (pre-treatment) and at 1, 2, 4, 6, and 8 weeks after treatment onset. Body weights were measured daily. Organ weights (liver, lungs, heart, and kidneys) were measured after eight weeks of treatment. All major organs and tissues (including brain and muscle) were subjected to pathological analysis. All tissues were fixed in a 10% zinc formalin solution overnight and stored in 70% ethanol for

histopathology evaluation. Serial tissue sections (5 μm each) were made, stained with hematoxylin and eosin (H&E), and examined histologically under a light microscope to assess any toxic effects of Mito-HNK.

Orthotopic lung cancer mouse model

We used an orthotopic model of lung cancer cells in non-obese/severe combined immunodeficiency (NOD/SCID) mice to evaluate the inhibitory effect of Mito-HNK on lung tumor growth. Five-week-old male NOD/SCID mice were used for these experiments. Mice were anesthetized with isoflurane and placed in the right lateral decubitus position. At eight weeks of age, H2030-BrM3 (NSCLC) or DMS-273 (SCLC) cells (1×10^6 cells/50 μg of growth factor-reduced Matrigel [BD Biosciences, San Jose, CA] in 50 μL of Waymouth's medium) were injected through the left rib cage of mice into the left lung, as previously described(*39*). One week later, mice were treated by oral gavage five days per week with HNK or Mito-HNK or vehicle (corn oil). Tumor growth was monitored by bioluminescence with the Xenogen IVIS-200 system. Mice were sacrificed at the endpoint, tissues were excised, freshly frozen, and OCT-fixed or formalin-fixed with 10% zinc for subsequent Western blot and immunohistochemistry (IHC) analyses.

Brain metastases generated in mice via an ultrasound-guided left ventricle injection

For the lung cancer brain metastasis study, 4–6-week-old female NOD/SCID mice were used. Brain-seeking H2030-BrM3 or DMS-273 cells (2×10^5) were suspended in PBS (0.1 mL) and injected into the left ventricle under ultrasound guidance (ECHO 707, GE,

Milwaukee, WI). One day after engrafting lung cancer cells in the arterial circulation, mice were randomly grouped into treatment groups: vehicle control (0.1% DMSO in corn oil), HNK, or Mito-HNK. Mice were treated by oral gavage five days per week and metastases were monitored periodically by bioluminescence using a Xenogen IVIS-200 system (Alameda, CA). At sacrifice, metastases were confirmed with *ex vivo* luminescence, *ex vivo* GFP fluorescence, and staining with H&E and with GFP protein immunostaining.

PathScan receptor Tyrosine kinase assay

H2030-BrM3 and DMS-273 cells were treated with vehicle control (DMSO), HNK or Mito-HNK for four hours and then lysed with a lysis buffer containing a proteinase inhibitor cocktail (Cell Signaling Technology, Danvers, MA), sheared 10 times by passage through a 28-gauge needle, and centrifuged at 16,000*g* for 30 min; the protein concentration of the supernatant was determined by the Bradford method. Lysates, normalized for equal protein loading, were analyzed by the PathScan RTK Signaling Array (Cell Signaling Technology, Danvers, MA) and the LI-COR Odyssey infrared imaging system (LI-COR Biosciences-Biotechnology, Lincoln, NE).

Western blot analysis

Cells were lysed with RIPA buffer containing a proteinase inhibitor cocktail (Fisher Scientific, Pittsburg, PA), sheared 10 times by passage through a 28-gauge needle, and centrifuged at 16,000 *g* for 30 min; the supernatants were normalized for protein concentration as determined by the Bradford method (*79*). Lysates were boiled for 5 min

and resolved on 4–12% sodium dodecyl sulfate polyacrylamide gel electrophoresis (SDS-PAGE) gels (Invitrogen, Carlsbad, CA). The blots were probed with the following primary antibodies from Cell Signaling Technology (Danvers, MA): p-EGFR-Tyr1068 (#3777S), p-STAT3-Tyr705 (#9131S), p-STAT3-Ser727 (#9134S), p-AKT-Ser473 (#4060S), EGFR (#4267S), STAT3 (#9139S), AKT (#9272S), or anti-actin (sc-8432, Santa Cruz Biotechnology, Dallas, TX).

Respiratory enzyme activity

Mitochondrial function was measured using a Seahorse XF96 Extracellular Flux Analyzer (Seahorse Bioscience, North Billerica, MA), as described previously (*3-5, 80*). For measurement of mitochondrial respiratory complexes, after 24-h treatments as indicated, intact cells were permeabilized using 1 nM Plasma Membrane Permeabilizer (PMP, Seahorse Bioscience) immediately before OCR measurement. The oxygen consumption derived from mitochondrial complex I or II activity was measured by providing different substrates to mitochondria, e.g., pyruvate/malate for complex I and succinate for complex II. Rotenone, malonate, and antimycin A were used as specific inhibitors of mitochondrial complex I, II, and III, respectively.

Analysis of intracellular oxidants

For analysis of the effect of the treatments on intracellular oxidant production, cells were treated for 24 h with the compound of interest, followed by 1-h incubation with hydroethidine (HE, 10 μM). After incubation, cells were harvested and the cell pellet stored at –80^{o}C until the day of HPLC analysis. Sample preparation and HPLC analysis

was performed as described previously (*81, 82*), with subsequent modifications (*83*). 2-hydroxyethidium was used as a specific marker for the superoxide radical anion, while diethidium was considered as a specific marker for one-electron oxidants(*84*).

Redox blots for peroxiredoxins

Redox Western blots for Prx1 and Prx3 were done as previously described (*85, 86*). Following treatment with Mito-HNK or vehicle control, cells were harvested to capture the protein thiol redox state: cells were washed once with Hank's Balanced Salt Solution (Life Technologies, Carlsbad, CA) and immediately scraped into *N*-ethylmaleimide (NEM) extract buffer (40 mM HEPES pH 7.4, 50 mM NaCl, 100 mM NEM, 1 mM EDTA, 1 mM EGTA, 1 mM PMSF, 10 µg/mL catalase). After 15 min at room temperature, the cells were pelleted (5 min, 800 *g*), and then lysed on ice in 35 µL NEM extract buffer containing 1% CHAPS (3-[(3-cholamidopropyl)dimethylammonio]-1-propanesulfonate). The lysates were held at –80°C until analysis. Lysates were thawed on ice and centrifuged for 5 min (8000 *g*, 4°C). The supernatants were run on non-reducing SDS-PAGE (NuPAGE Novex 10% Bis-Tris gels), and the blots were probed with anti-Prx1 (sc-7381) or anti-Prx3 (sc-59661 or sc-59663) (all from Santa Cruz Biotechnology), followed by the appropriate HRP-conjugated secondary antibody. The blots were developed using SuperSignal West Pico Chemiluminescent Substrate (Thermo Scientific, Rockford, IL). Multiple exposure times were captured, and the percent of oxidized vs. reduced Prx was determined by image densitometry using UN-SCAN-IT software v.6.1 (Silk Scientific, Orem, UT).

Live cell imaging

Cells (parental or ρ0) growing on glass cover slides (VWR) in 6-well plates were evaluated for mtDNA depletion by live cell imaging as previously described (*87*). Cells were stained with PicoGreen (3 µl/ml; Invitrogen) for 1 h at 37°C to visualize mtDNA, MitoTracker Deep Red (1 μM; Invitrogen) was added and the cells were incubated for a further 20 min. After three washes with cold PBS, cells were visualized and photographed with a Zeiss SP5 confocal microscope using a 63x oil immersion objective.

Endogenous STAT3 knockdown and KO using CRISPR System

STAT3 shRNA lentiviral particles purchased from Santa Cruz Biotechnology, Inc., were used in the presence of 8 µg/mL polybrene to infect PC9-BrM3, H2030-BrM3, and DMS-273 cells. The infected cells were selected with puromycin (2 µg/mL) for three days to obtain stable knockdown cells. To generate complete knockouts of STAT3, the bicistronic pX330 vector containing cDNAs encoding human codon-optimized *Streptococcus pyogenes* Cas9 (hSpCas9) and an adaptable CRISPR RNA (crRNA)/trans-activating crRNA chimera containing adjacent *Bbs*I cloning sites for protospacer “guide sequence” insertion was purchased from Addgene (plasmid no. 42230). Three guide sequences targeting DNA within the first exon of STAT3 were selected from the online design site. After annealing, the oligos were ligated into the *Bbs*I-digested pX330 vector. After cloning and polymerase chain reaction (PCR) validation, we used the Cel-1 assay in HEK-293 cells to authenticate the cleavage of the STAT3 gene (**Supplementary Fig. 8**). The correct construct(s) that can successfully

cleave the target gene were then transfected into H2030-BrM3 cells, along with a puromycin transgene targeted to the AAVS1 safe harbor locus (Systems Biosciences, Palo Alto, CA) to establish puromycin-resistant clones. Each individual clone was then screened by PCR and DNA sequencing (**Supplementary Fig. 8**), and the knockouts were validated by Western blot. Two CRISPR-STAT3 knockout colonies had frameshift mutations, resulting in total STAT3 knockout (**Supplementary Fig. 8**).

Species-Specific RNAseq

Total RNA was extracted from the H2030-BrM3 brain metastatic lesions of nude mice treated with Mito-HNK or vehicle control for four weeks (n=3 per group), as described above. Total RNA (4 µg) was poly-A purified, transcribed, and chemically fragmented using Illumina's TruSeq RNA library kit, per the manufacturer's protocol. Individual libraries were prepared for each sample, indexed for multiplexing, and then sequenced on an Illumina HiSeq 2000 (Illumina, Inc., San Diego, CA). Sequences for all RNA transcripts were annotated using the human build GRCh37 and mouse build MGCSv37 and were then concatenated to create a joint human and mouse transcriptome reference. Reads of each xenograft sample were aligned to the joint transcriptome references using Bowtie2 (*88*). Default parameters were used with the exception of a Bowtie2 offset of 1, trading index size for increased alignment speed. Expression abundances were quantified at the whole transcript-level as effect counts using eXpress version 1.5.1 (*89*). The transcript-level count data were aggregated per gene and rounded to integer to produce gene-level count matrix. Differential expression (DE) analysis was performed with the DESeq2 (*90*) to compute log2 fold changes and FDR-

adjusted p-values. Statistical significance was determined at an FDR threshold of 0.05. DE analysis was carried out separately for mouse and human to allow for normalization of different relative contributions of malignant tumor cells and the nonmalignant host stroma. Species-Specific RNAseq (SSRS) data were analyzed for molecular and functional pathway enrichment using the Ingenuity IPA tool (Qiagen, Redwod City, CA).

Data and statistical analysis

To compare multiple groups, one-way analysis of variance (ANOVA) was used followed by Dunnett's post-hoc test. **P*<0.05, ***P*<0.01, and ****P*<0.001 were considered statistically significant and marked accordingly. Mice were randomly assigned to the treatment groups, and the duration that mice were followed for each experiment is shown in each figure legend section.

Synthesis of mitochondria-targeted analogs of honokiol.

General. All chemicals and organic solvents were commercially available and were used as supplied. The reactions were monitored by TLC using silica gel Merck ^{60}F254. Crude materials were purified by flash chromatography on Merck Silica gel 60 (0.040-0.063 mm). ^{1}H NMR spectra were recorded at 400.13 MHz using a Bruker DPX AVANCE 400 spectrometer equipped with a QNP probe. ^{1}H NMR and ^{31}P were taken in $CDCl_3$ using $CDCl_3$ and TMS as internal reference, respectively. Chemical shifts (□) are reported in ppm and *J* values in Hertz.

10-Bromodecyltriphenylphosphonium bromide 1. A mixture of triphenylphosphonium (1 g, 3.8 mmol) and dibromide (5.7 g, 19 mmol) was heated at 90°C for 6 h. After cooling, the crude product was purified by flash chromatography (Pentane, Et_2O and CH_2Cl_2/EtOH 9:1) to afford the corresponding phosphonium salt **1** as a white solid (1 g, 47% yield).

^{31}P (400.13 MHz, $CDCl_3$) □ 24.32. ^{1}H NMR (400.13 MHz, $CDCl_3$) □□7.85-7.65 (15H, m), 3.73-3.66 (2H, m), 3.40-3.34 (2H, m), 1.80-1.75 (4H, m), 1.31-1.20 (12H, m).

***Mono*-mito-honokiols** ({10-[3',5-diallyl-4'-hydroxy-(1,1'-biphenyl)-2-yl]-oxy}-decyltriphenylphosphonium **[2]** and {10-[3,5'-diallyl-2'-hydroxy-(1,1'-biphenyl)-4-yl]-oxy}-decyltriphenylphosphonium **[3]**) **and *bis*-mito-honokiol** ([3',5-diallyl-(1,1'-biphenyl)-2,4'-diyl]-bis-(oxy)-bis-(decane-10,1-diyl)-bis-(triphenylphosphonium) **[4]**). To a mixture of honokiol (0.27 g, 2.6 mmol), anhydrous potassium carbonate (0.28, 2 mmol) in DMF (4 mL) was added to compound **1** (0.57, 1.0 mmol). The mixture was stirred at 30 °C for 6h. The solvent was removed under vacuum and the residue was taken up into water and extracted with CH_2Cl_2. The organic layer was dried over Na_2SO_4, and the solvent was removed under reduced pressure. Purification by flash chromatography (Et_2O, CH_2Cl_2 and CH_2Cl_2/EtOH) delivered the corresponding *mono*-mito-honokiols as a mixture of two isomers **2**, **3** and the *bis*-mito-honokiol **4** as white solids (**2**, **3**, 250 mg, 33 % yield; and **4**, 100 mg, 10 % yield). HRMS calculated for **2**, **3** $C_{46}H_{52}O_2P$ $[MH]^+$ 667.3699, found, 667.3699. HRMS calculated for **4** $C_{74}H_{86}O_2P_2$ $[MH]^{2+}$ 534.3046, found, 534.3044.

***Mono*-mito-honokiol 2, 3.** ^{31}P (400.13 MHz, $CDCl_3$) □ 24.38, 24.28. ^{1}H NMR (400.13 MHz, $CDCl_3$) □ 7.86-7.65 (15H, m), 7.35-6.95 (5H, m), 6.87 (1H, 2d, *J* = 8.3, 8.5), 6.06-5.86 (2H, m), 5.10-4.93 (4H, m), 3.98 (1H, t, *J* = 3.9), 3.89 (1H, t, *J* = 3.8), 3.80-3.70 (2H, m), 3.4-3.33 (4H, m), 1.77-1.30 (10H, m), 1.1-1.07 (6H, m).

***Bis*-mito-honokiol 4.** ^{31}P (400.13 MHz, $CDCl_3$) □□ 24.37. ^{1}H NMR (400.13 MHz, $CDCl_3$) □ 7.88-7.70 (30H, m), 7.35-7.32 (2H, m), 7.12 (1H, d, *J* = 1.7), 7.07 (1H, dd, *J* = 8.3, 2.0), 6.88 (1H, d, *J* = 8.3), 6.85 (1H, d, *J* = 8.3), 6.05-5.85 (2H, m), 5.13-4.93 (4H, m), 3.97 (2H, t, *J* = 6.3), 3.90 (2H, t, *J* = 6.3), 3.85-3.73 (4H, m), 3.39 (2H, d, *J* = 6.8), 3.36 (2H, d, *J* = 6.5), 1.71-1.50 (10H, m), 1.20-1.33 (22H, m).

<u>Mass spectrometry analysis of mitochondria-targeted analogs of honokiol.</u>

HRMS calculated for **2**, **3** $C_{46}H_{52}O_2P$ $[MH]^+$ 667.3699, found, 667.3699. HRMS calculated for **4** $C_{74}H_{86}O_2P_2$ $[MH]^{2+}$ 534.3046, found, 534.3044.

Fig. S1

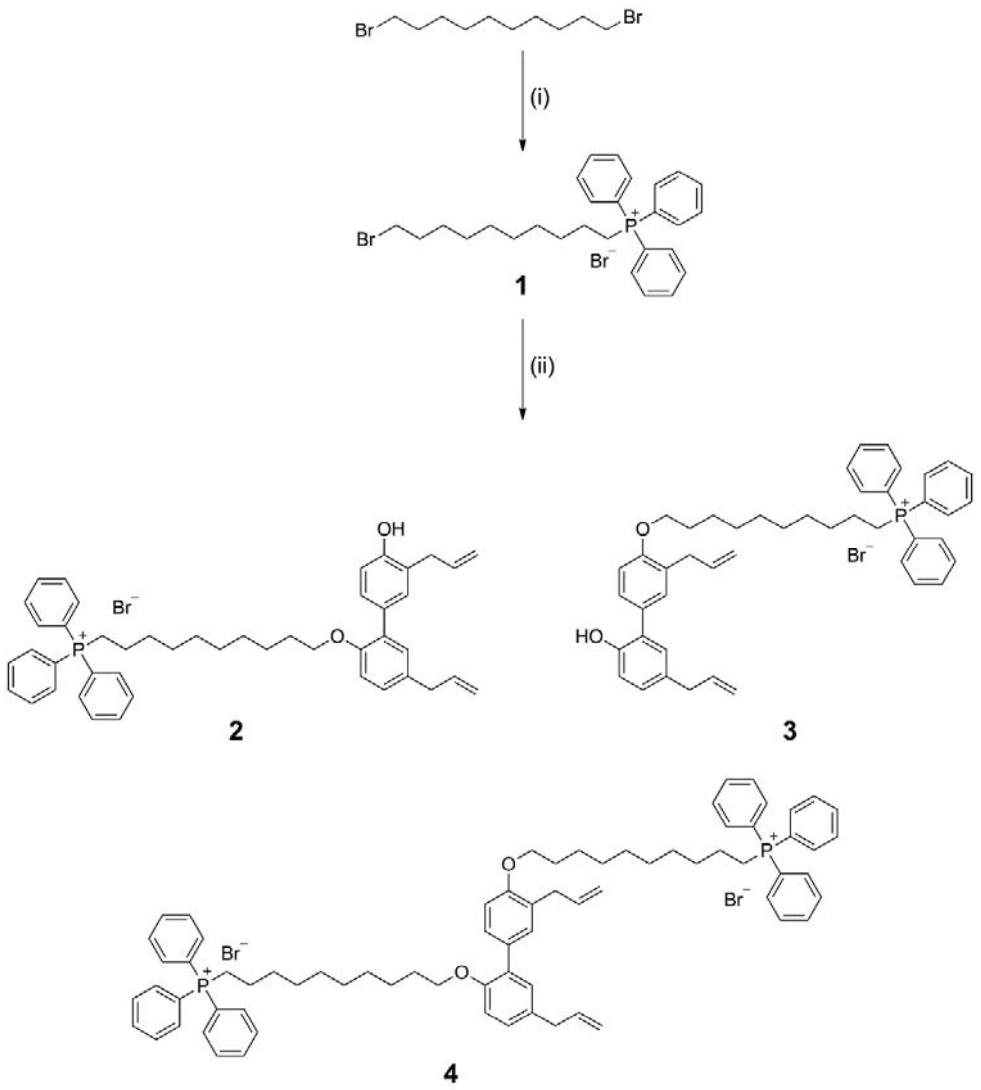

Fig. S1. Synthesis of mitochondria-targeted honokiols (mito-honokiols). Reagents and conditions: i, PPh_3, neat, 6 h, 90°C, 47%; ii, Honokiol, K_2CO_3, DMF, 43%.

Fig. S2

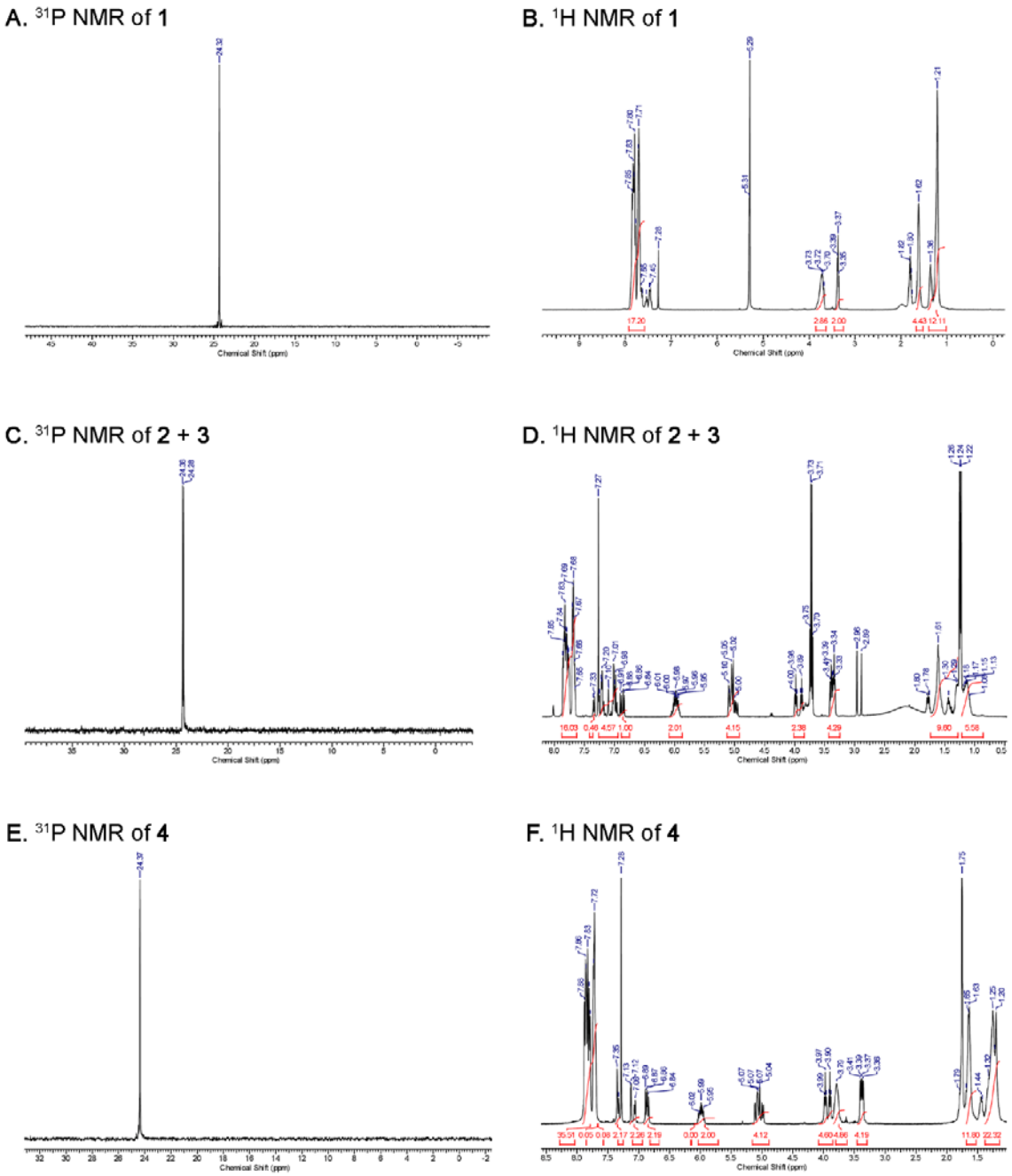

Fig. S2. NMR spectra of synthesized compounds 1, 2+3 and 4. (**A**) ^{31}P NMR spectrum (400.13 MHz, $CDCl_3$) of compound **1**; (**B**) ^{1}H NMR spectrum (400.13 MHz, $CDCl_3$) of compound **1**; (**C**) and (**D**) same as panels (**A**) and (**B**) but for *mono*-mito-honokiol (compounds **2** + **3**); (**E**) and (**F**) same as panels (**A**) and (**B**) but for *bis*-mito-honokiol (compound **4**).

Fig. S3

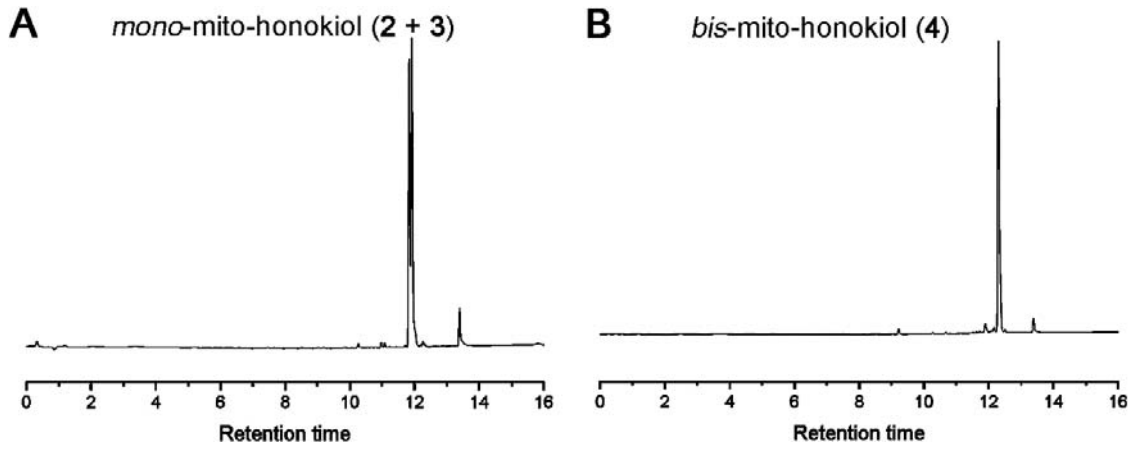

Fig. S3. HPLC analysis of mitochondria-targeted analogs of honokiol. (**A**) Analysis of *mono*-mito-honokiol. Double peak indicates of the presence of two isomers. (**B**) Analysis of *bis*-mito-honokiol. HPLC experiments were performed using an Agilent 1200 system equipped with UV-Vis absorption and fluorescence detectors using a C_{18} column (Phenomenex, Kinetex C_{18}, 100 mm × 4.6 mm, 2.6 μm) that was equilibrated with 10% CH_3CN (containing 0.1% (v/v) trifluoroacetic acid (TFA) in 0.1% TFA aqueous solution. Five minutes after injection, the CH_3CN fraction was increased to 40%; 10 min after injection, the CH_3CN fraction was increased to 100% until 16 min. The compounds were eluted using a flow rate of 1.5 ml/min.

Fig. S4

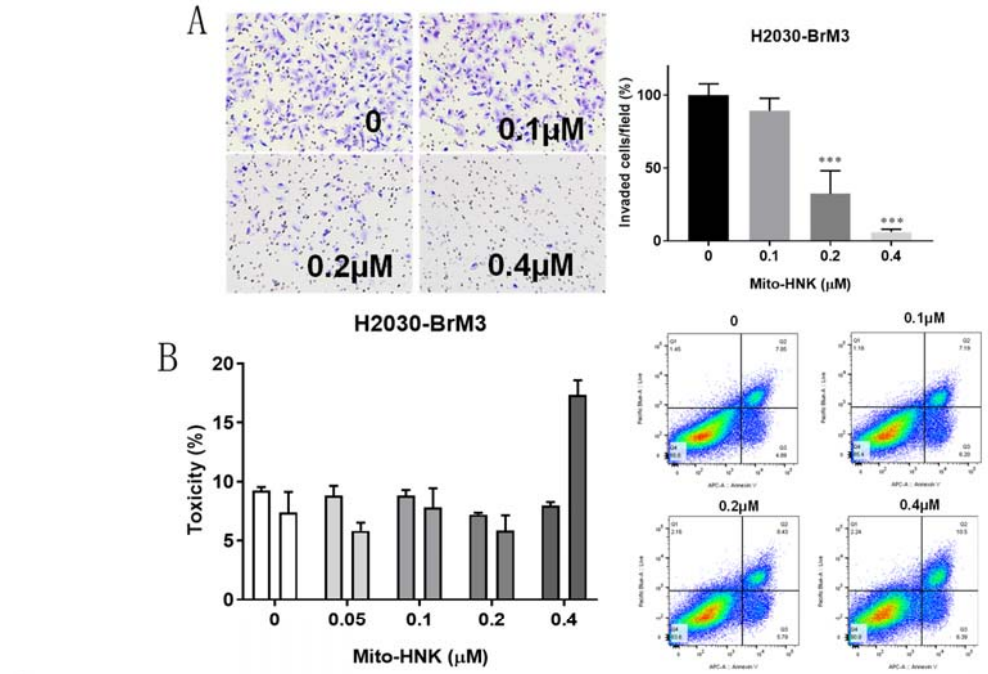

	%G1	%S	%G2
Ctrl	54.8	25.4	20.1
Mito-HNK-0.2μM	59.0	22.9	18.5
Mito-HNK-0.4μM	64.3	21.5	15.1

Fig. S4. Mito-HNK inhibits invasion without induction of significant cell death in lung cancer cells. (**A**) Pretreat with Mito-HNK inhibits invasion of lung cancer cells. To rule out the pro-apoptotic effects of mito-HNK, lung cancer cells H2030-BrM3 were pretreated with different doses of mito-HNK for 24 hours, then mito-HNK was washed out, cells were trypsinzed and plated in the Boyden chamber for invasion assay. Representative images are shown in left panel and the quantitative data are in the right panel. (**B**) Mito-HNK does not cause cells death at low doses. Lung cancer cells were treated with different doses of mito-HNK for 24 or 48 hr, supernatant was collected and subjected for LDH cytotoxicity assay following manufacturer's instruction. (**C**) Mito-HNK blocks cell cycle.

Fig. S5

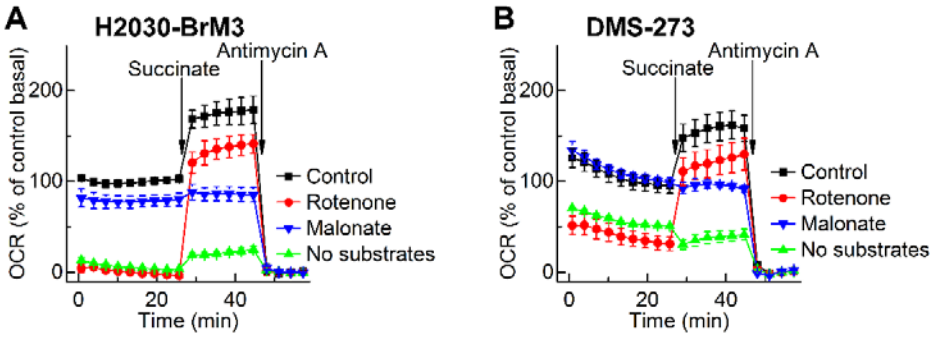

Fig. S5. Experimental setup for measurement of mitochondrial complex I and II activities in permeabilized cells. H2030-BrM3 (**A**) or DMS-273 (**B**) cells were permeabilized and assayed in medium containing 10 mM pyruvate and 1.5 mM malate (substrates for complex I) in mannitol and sucrose (MAS) buffer using the Seahorse XF96 analyzer. Either rotenone (1 μM, complex I inhibitor) or malonate (10 mM, complex II inhibitor) was added immediately before starting the measurements of oxygen consumption rate (OCR). Both succinate (10 mM, substrate for complex II) and antimycin A (20 μM, complex III inhibitor) were injected as indicated.

Fig. S6

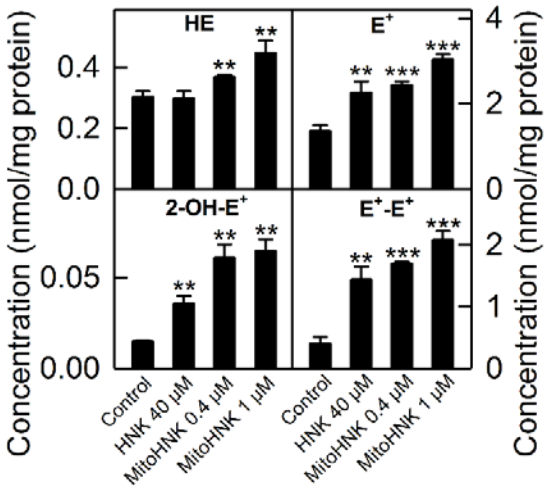

Fig. S6. The effect of HNK and Mito-HNK (24 h treatment) on cellular ROS production, as measured by HPLC-based profiling of the oxidation products of the HE probe in H2030-BrM3 cells. 2-hydroxyethidium (2-OH-E^+) is used as a specific product for superoxide, and diethidium (E^+-E^+) as a marker product for one-electron oxidants. **$p < 0.01$, ***$p < 0.001$.

Fig. S7.

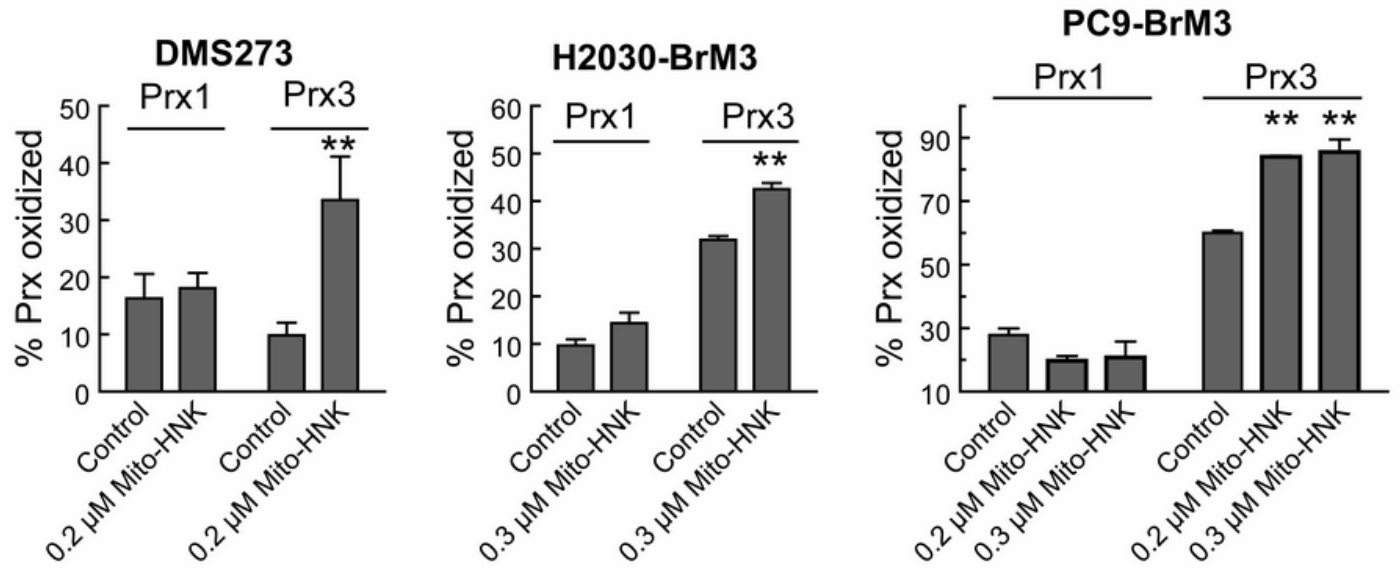

Fig. S7. Effect of Mito-HNK on the oxidation status of cytosolic (Prx1) and mitochondrial (Prx3) peroxiredoxins in three different lung cancer cell lines. Cells were treated with the indicated concentrations of Mito-HNK for 24 h and the redox status of peroxiredoxins determined, as described in the experimental section.

Fig. S8.

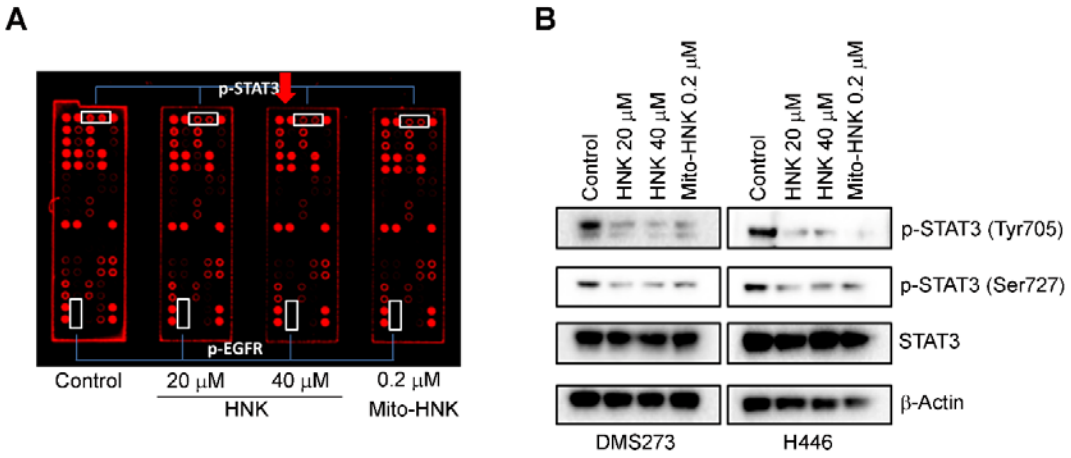

Fig. S8. Role of STAT3 in the anti-proliferative and anti-invasive effects of HNK and Mito-HNK in small cell lung cancer cells. **A.** Results of receptor tyrosine kinase proteomic array of DMS-273 SCLC cells treated with HNK (20 μM) or Mito-HNK (0.2 μM) for 24 h. **B.** Western blot analysis showing the effect of HNK and Mito-HNK on STAT3 phosphorylation status in DMS-273 and H446 SCLC cells.

Fig. S9

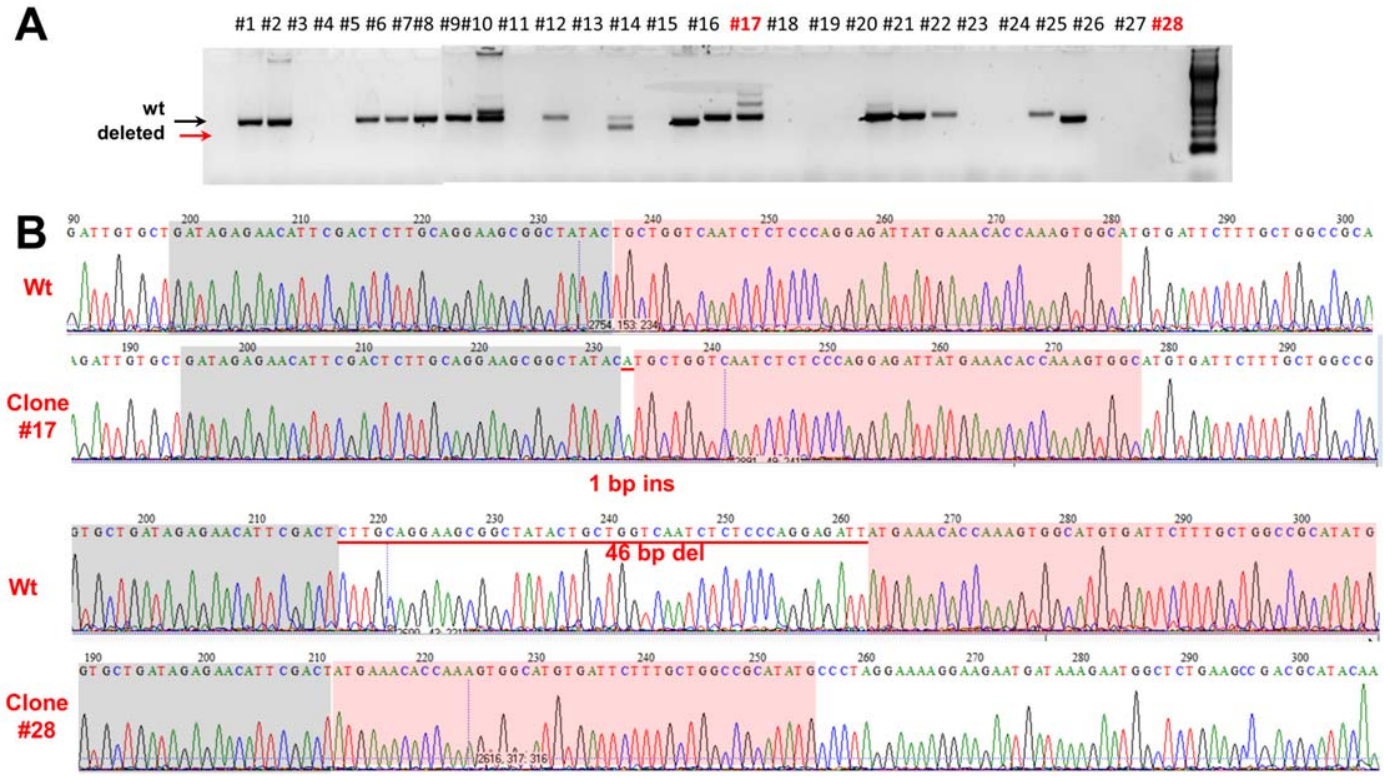

Fig. S9. Generation and validation of STAT3 knockout H2030-BrM3 cell line. (**A**) Cel-1 assay, a mismatch-specific endonuclease assay. Genomic PCR (gPCR) products spanning exon 1 of *STAT3 gene* were amplified from the template of a heterogeneous population of HEK293T cells transfected with px330-STAT3 guide. Rehybridization and treatment with Cel1 nuclease resulted in fallout bands of ~150–250 bp, shown by arrows. This is consistent with the predicted cleavage sizes of 251 bp and 176 bp. (**B**) After clone isolation, PCR amplicons of clonal STAT3 KO isolates (*clone 17* and *clone 28*) encompassing the modified locus of genomic DNA were sequenced which shows that clone #17 contains a 1-bp insertion, and #28 contains a 46-bp deletion in both alleles.

Fig. S10

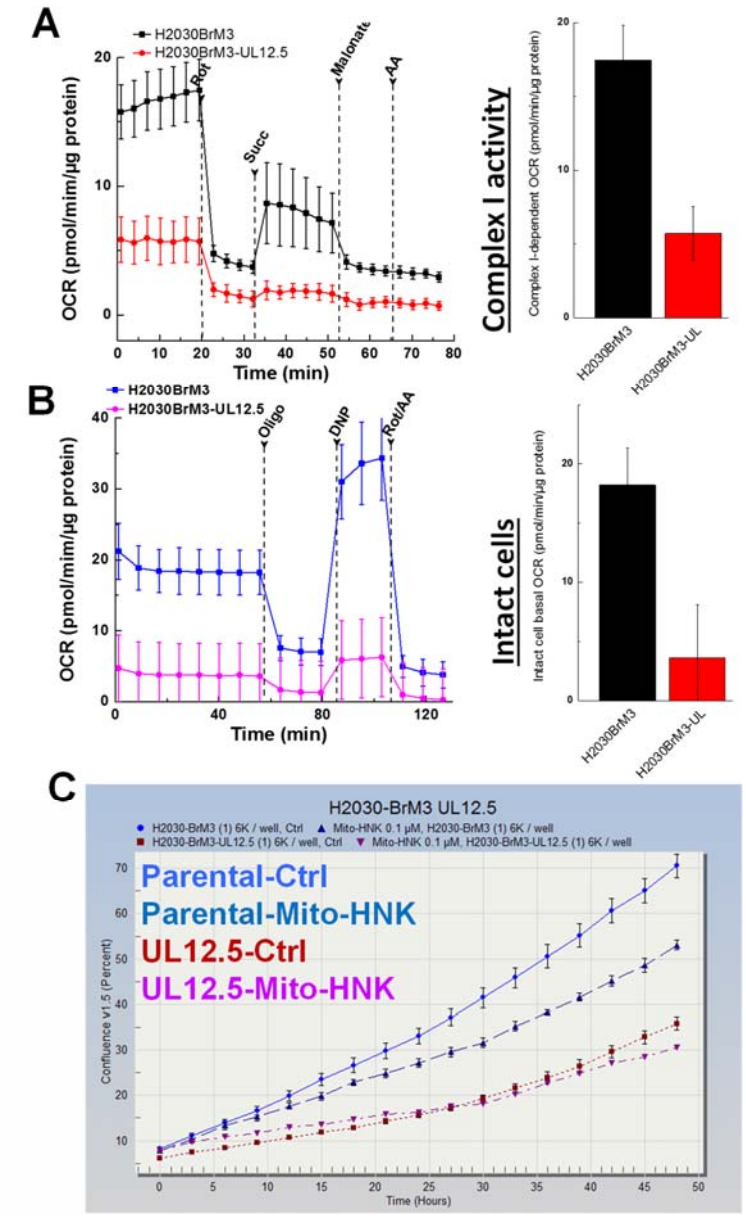

Fig. S10. Eliminate mtDNA with Herpes simplex virus UL12.5 abrogates anti-proliferative effects of Mito-HNK in lung cancer cells. (A,B) Loss of mitochondrial function was seen in UL12.5 transfected H2030-BrM3 cells as evidenced by very low levels for complex I-dependent OCR and intact cell OCR. **(C)** UL12.5 transfected H2030-BrM3 cells are more resistant to Mito-HNK treatment, indicating that mitochondria are an important target for Mito-HNK.

Fig. S11

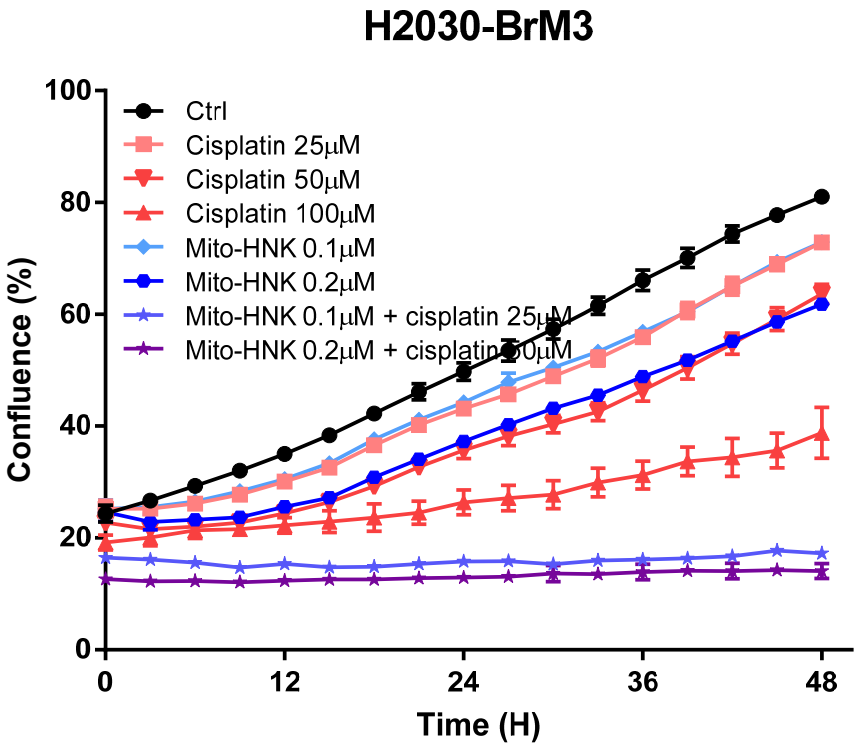

Fig. S11. Combination of Mito-HNK with cisplatin increased anti-proliferative effects in lung cancer cells. H2030-BrM3 cells were treated with mito-HNK alone or in combination with cisplatin, confluency was monitored using Incucyte every three hours,

Table. S1. Modified Irwin screen after 8-week Mito-HNK treatment. Values reflect the mean ± SEM of the deviation score (0=normal, 1=mild deviation, 2=moderate deviation, 3=extreme deviation) or metric noted for each attribute after 8-week treatment with Mito-HNK or vehicle. Observations were conducted by two different experimenters and the scores were averaged.

	Mito-HNK Dose			
	vehicle	**2x**	**10x**	**20x**
Physical condition				
Body weight (g)	22.0±0.8	21.8±0.4	20.8±1.3	20.8±1.0
Rectal temperature (ºC)	35.2±0.8	34.0±0.5	34.2±0.3	34.0±0.4
Presence of whiskers	0.0±0.0	0.0±0.0	0.0±0.0	0.0±0.0
Well-groomed	0.0±0.0	0.0±0.0	0.0±0.0	0.0±0.0
Piloerection	0.6±0.2	0.4±0.2	0.8±0.3	0.0±0.0
Fur missing on face	0.0±0.0	0.0±0.0	0.0±0.0	0.0±0.0
Fur missing on body	0.0±0.0	0.0±0.0	0.0±0.0	0.0±0.0
Wounds	0.0±0.0	0.0±0.0	0.0±0.0	0.0±0.0
Skin color	0.0±0.0	0.0±0.0	0.0±0.0	0.0±0.0
Palpebral closure	0.2±0.2	0.0±0.0	0.0±0.0	0.0±0.0
Behavior in novel environment				
Transfer behavior	1.4±0.2	1.8±0.2	1.3±0.3	1.2±0.2
Body positioning	0.0±0.0	0.0±0.0	0.3±0.3	0.0±0.0
Spontaneous activity	0.0±0.0	0.0±0.0	0.0±0.0	0.0±0.0
Respiration rate	0.8±0.2	0.6±0.2	0.5±0.3	0.2±0.2
Tremor	0.0±0.0	0.0±0.0	0.0±0.0	0.0±0.0
Piloerection	1.0±0.0	0.6±0.2	0.8±0.3	0.4±0.2
Gait	0.0±0.0	0.0±0.0	0.0±0.0	0.0±0.0
Pelvic elevation	0.2±0.2	0.4±0.2	0.0±0.0	0.2±0.2
Tail elevation	0.0±0.0	0.0±0.0	0.0±0.0	0.0±0.0
Urination	0.0±0.0	0.0±0.0	0.0±0.0	0.0±0.0
Defecation	0.4±0.2	0.4±0.2	0.0±0.0	0.0±0.0
Reflexes or reaction to stimuli				
Touch escape	0.8±0.2	1.0±0.0	1.0±0.0	0.8±0.2
Positional passivity	1.2±0.2	1.0±0.0	1.5±0.3	1.0±0.0
Trunk curl	0.0±0.0	0.0±0.0	0.0±0.0	0.0±0.0
Reaching reflex	0.0±0.0	0.0±0.0	0.0±0.0	0.0±0.0
Pinna reflex	0.0±0.0	0.0±0.0	0.0±0.0	0.0±0.0
Preyer reflex at ~90 dB	0.6±0.2	0.8±0.2	0.8±0.3	0.0±0.0
Toe pinch response	0.0±0.0	0.0±0.0	0.0±0.0	0.0±0.0
Righting reflex	0.0±0.0	0.0±0.0	0.0±0.0	0.0±0.0
Air righting reflex	0.0±0.0	0.0±0.0	0.0±0.0	0.0±0.0
Inverted screen latency to fall (s)	49.2±10.1	50.8±5.6	49.0±11.0	60.0±0.0
Provoked biting	1.0±0.0	1.0±0.0	1.0±0.0	1.0±0.0
Measures during supine restraint				
Limb tone	0.2±0.2	0.0±0.0	0.3±0.3	0.0±0.0
Abdominal tone	0.8±0.2	0.6±0.2	0.3±0.3	0.4±0.2
Toe pinch	0.0±0.0	0.0±0.0	0.0±0.0	0.0±0.0

Values reflect the mean ± SEM of the deviation score (0=normal, 1=mild deviation, 2=moderate deviation, 3=extreme deviation) or metric noted for each attribute after 8-week treatment with Mito-HNK or vehicle. Observations were conducted by two different experimenters and the scores were averaged.

Table. S2. Gene expression in malignant tumor cells from brain metastatic lesions of mice treated with Mito-HNK or vehicle control (Attached Excel file: **Table. S2.xlsx**)

Table. S3. Gene expression in nonmalignant stromal cells from brain metastatic lesions of mice treated with Mito-HNK or vehicle control (Attached Excel file: **Table. S3.xlsx**)